Article

# Driving Forces for Self-Organized Coadsorption: CH/2O and CH/2CO on Ni{111}

S. Yamagishi, S. J. Jenkins, and D. A. King

*J. Am. Chem. Soc.*, **2004**, 126 (35), 10962-10971• DOI: 10.1021/ja048289y • Publication Date (Web): 14 August 2004

J|A|C|S
ARTICLES
Published on Web 08/14/2004

# Driving Forces for Self-Organized Coadsorption: $C_6H_6$/2O and $C_6H_6$/2CO on Ni{111}

S. Yamagishi,[†] S. J. Jenkins,[‡] and D. A. King*[,‡]

*Contribution from the National Metrology Institute of Japan (NMIJ), National Institute of Advanced Industrial Science and Technology (AIST), Japan, and Department of Chemistry, University of Cambridge, Lensfield Road, Cambridge, CB2 1EW, UK*

Received March 25, 2004; E-mail: daksec@ch.cam.ac.uk

***Abstract:*** The self-organized ($2\sqrt{3} \times 2\sqrt{3}$) coadsorbed phases of $C_6H_6$ with O and with CO are investigated within first-principles density functional theory. The main driving force for formation of the $C_6H_6$/2O phase is found to be the reduction of O adatom repulsive interactions, while for the $C_6H_6$/2CO phase it is the interspecies attractive interactions and benzene−benzene repulsive interactions which are most important.

## I. Introduction

Self-organizing systems are the focus of much current attention, in light of their significance for possible nanotechnological applications. The painstaking assemblage of functional units to achieve a complex purpose seldom represents a viable mode of nanomanufacture, so the concept of diverse molecular components which will automatically find their correct place in a device is clearly an appealing proposition. In fact, the spontaneous emergence of order in molecular systems is a phenomenon frequently observed in surface science, where overlayers of a single molecular species often adopt ordered structures commensurate with an underlying metallic substrate. One would not ordinarily consider such systems to be self-organized, however, as an ordered array of identical components is essentially trivial from a nanotechnological standpoint.

Coadsorption of multiple species, on the other hand, opens a door to a range of possibilities: the species may mix intimately in a disordered fashion, segregate to form single-species islands or indeed react to produce entirely different species on the surface. In a small number of cases, however, the coadsorbed species can self-organize, adopting a structure which is both intimately mixed and well-ordered. While it remains far from clear to what extent these structures may be exploited, it is certain that a first step toward useful devices must be to gain an understanding of the driving forces which dictate the tendency toward self-organization. We believe that density functional theory (DFT), together with crystallographic measurements, can fruitfully be employed to address this issue. To that end, we report here on calculations aimed at an understanding of two related systems, in which benzene is coadsorbed with either O adatoms or CO molecules to form a self-organized overlayer.

As the prototypical aromatic compound, benzene has attracted considerable attention as an adsorbate on transition metal surfaces. Most frequently found to adsorb with its ring parallel to the surface, it exhibits only relatively small energy differences between different possible sites and orientations, leading to a tendency toward the formation of disordered overlayers. Only on a few substrates, such as Ni{111} and Ru{0001}, will an ordered monolayer be formed. Intriguingly, however, it has been reported[1] that long-range ordered structures of benzene are more readily formed under the influence of small amounts of coadsorbates, such as O or CO.

Coadsorption of benzene with O on Ni{111} leads to a well-ordered ($2\sqrt{3} \times 2\sqrt{3}$)*R*30° structure. Angle-resolved ultraviolet photoemission spectroscopy (ARUPS) suggests that the molecule is adsorbed with its H atoms pointing along the [$\bar{2}$11] directions of the substrate[2] (hereafter simply referred to as the "[$\bar{2}$11] orientation", as opposed to the alternative "[$\bar{1}$10] orientation"). Furthermore, a low-energy electron diffraction (LEED) study[3] has shown that both the benzene molecule and the O adatoms occupy the *fcc* hollow sites of the substrate, although a [$\bar{1}$10] orientation was favored in contradiction to the ARUPS work. Coadsorption of benzene with CO on Ni{111} similarly leads to a well-ordered ($2\sqrt{3} \times 2\sqrt{3}$)*R*30° structure, with ARUPS again indicating flat-lying benzene in the [$\bar{2}$11] orientation.[2,4] A recent LEED study[5,6] revealed that both molecules were adsorbed on the *hcp* hollow sites, in contrast to the case of O coadsorption, and also favored the [$\bar{2}$11] orientation.

In both cases, some interaction between the benzene and its coadsorbates may be expected to influence the formation of the ordered monolayer. It should be noted that the same coverage of benzene *without* coadsorbates is characterized by disordered occupation of the bridge sites.[7] The aim of the present work is

[†] National Metrology Institute of Japan (NMIJ).
[‡] University of Cambridge.

(1) Mate, C. M.; Somorjai, G. A. *Surf. Sci.* **1985**, *160*, 542.
(2) Huber, W.; Zebisch, P.; Bornemann, T.; Steinrück, H.-P. *Surf. Sci.* **1991**, *258*, 16.
(3) Titmuss, S. Ph.D. Thesis, University of Cambridge, 1999.
(4) Huber, W.; Steinrück, H.-P.; Pache, T.; Menzel, D. *Surf. Sci.* **1989**, *217*, 103.
(5) Braun, W. Ph.D. Thesis, University of Erlangen, 2003.
(6) Braun, W.; Steinrück, H-P.; Held, G. In preparation.


**10.1021/ja048289y CCC: $27.50** 

to study the $(2\sqrt{3} \times 2\sqrt{3})R30°$ coadsorbed phases of benzene with O and with CO on Ni{111} with a view to elucidating these influences through consideration of atomic geometry and electronic structure. The technique employed is a first-principles, periodic implementation of the density functional theory (DFT) of Hohenberg, Kohn, and Sham.[8,9]

## II. Methodology and Reference Calculations

The present calculations were performed by means of the CASTEP computer code,[10] using ultrasoft pseudopotentials[11] and a plane wave basis set of 340 eV cutoff. Electronic exchange and correlation were included through the generalized gradient approximation (GGA) in the Perdew−Wang form (PW91),[12] and the Brillouin zone of the $(2\sqrt{3} \times 2\sqrt{3})R30°$ unit cell was sampled via a $2 \times 2 \times 1$ Monkhorst−Pack mesh[13] of *k*-points. In view of the ferromagnetism of the Ni{111} surface, we have performed spin-polarized calculations for the system. These spin-polarized calculations require the use of a Ni pseudopotential incorporating nonlinear core corrections (NLCC)[14] in order correctly to describe the surface magnetism.[15]

All convergence-related parameters used in the present work were fully consistent with those employed for our previous studies of benzene,[16] CO,[17] and O[18] on Ni{111}. In particular, the validity of the cutoff energy and mesh density were inferred from test calculations on bulk Ni, in which we obtained a lattice constant of 3.55 Å, in good agreement with the experimental value[19] of 3.524 Å. The C−C and C−H bond lengths of free benzene were calculated as 1.38 and 1.08 Å, again in good agreement with the respective experimental values[19] of 1.399 and 1.101 Å. The C−O bond length of the free CO molecule was also calculated to be 1.14 Å, in good agreement with the experimental value[19] of 1.1283 Å.

The surface calculations themselves were performed for a four-layer Ni slab with vacuum region equivalent to nine Ni layers and adsorbates placed on only one side of the slab. The structures of the adsorbates and of the top two surface layers were relaxed according to the calculated forces, with the back two layers of the slab held fixed in their ideal bulk geometry. Localized information embedded in the electron and spin densities was subsequently extracted from the plane wave results by means of a topological technique due to Bader.[20]

In view of the large size of this system, we initially guessed the possible adsorption sites of the benzene molecule and its coadsorbates by referring to separate calculations of the pure benzene, pure O, and pure CO adsorbate phases. In the case of benzene coadsorbed with O, we referred to our previous calculations of benzene on Ni{111} in the $(\sqrt{7} \times \sqrt{7})$ unit cell[16] and of O on Ni{111} in the $(\sqrt{3} \times \sqrt{3})$ unit cell.[18] The distinct preference of O for adsorption in either the *hcp* or the *fcc* site (the *bridge* and *atop* sites are unstable for O on Ni{111}) is expected to drive both components of the coadsorption system toward occupation of hollow sites. Simply combining the calculated adsorption energies for the separate systems (Table 1), we arrive at a measure of the stability of a putative two-phase system in which the two different species form distinct islands on the surface rather than an intimately mixed coadsorbed phase. The resulting adsorption energy per ($C_6H_6$ + 2O) unit, relative to the gas-phase molecular species, falls in the range 4.77−5.01 eV for hollow site models but is only 4.05 eV for the [$\bar{2}$11] *bridge* model. Spin-relaxed *atop* and [$\bar{1}$10] *bridge* models were never calculated in our previous study for the $(\sqrt{7} \times \sqrt{7})$ benzene overlayer, as preliminary zero-spin calculations had shown them to be much higher in energy than the hollow models. We do not, therefore, list two-phase adsorption energies for these cases but nevertheless expect them to be significantly unfavorable. We conclude from these considerations that *atop* and *bridge* models may safely be excluded from our coadsorption studies but that the range of the two-phase adsorption energies for the *fcc* and *hcp* models is sufficiently narrow that all four corresponding coadsorption models must be investigated in detail.

***Table 1.*** Comparison of Two-Phase and Intimately Coadsorbed Adsorption Energies (in eV) per ($C_6H_6$ + 2O) Unit, Relative to the Gas-Phase Molecular Species[a]

| adsorption site | $C_6H_6$ orientation | $(\sqrt{7}\times\sqrt{7})$ Ni{111}/$C_6H_6$ | $(\sqrt{3}\times\sqrt{3})$ Ni{111}/O | two-phase | $(2\sqrt{3}\times2\sqrt{3})$ coadsorbed |
|---|---|---|---|---|---|
| fcc | [$\bar{1}$10] | 0.79 | 2.11 | 5.01 | 6.14 |
| fcc | [$\bar{2}$11] | 0.67 | 2.11 | 4.89 | 6.02 |
| hcp | [$\bar{1}$10] | 0.79 | 2.02 | 4.83 | 5.96 |
| hcp | [$\bar{2}$11] | 0.73 | 2.02 | 4.77 | 5.87 |
| bridge | [$\bar{1}$10] | | 1.57 | | |
| bridge | [$\bar{2}$11] | 0.91 | 1.57 | 4.05 | |
| atop | [$\bar{1}$10] | | 0.36 | | |
| atop | [$\bar{2}$11] | | 0.36 | | |

[a] The two-phase adsorption energy is defined as the sum of the adsorption energies of Ni{111}/$C_6H_6$-$(\sqrt{7} \times \sqrt{7})$ [ref 16] and $2 \times$ Ni{111}/O-$(\sqrt{3} \times \sqrt{3})$ [ref 18].

***Table 2.*** Comparison of Two-Phase and Intimately Coadsorbed Adsorption Energies (in eV) per ($C_6H_6$+2CO) Unit, Relative to the Gas-Phase Molecular Species[a]

| adsorption site | $C_6H_6$ orientation | $(\sqrt{7}\times\sqrt{7})$ Ni{111}/$C_6H_6$ | $(\sqrt{3}\times\sqrt{3})$ Ni{111}/CO | two-phase | $(2\sqrt{3}\times2\sqrt{3})$ coadsorbed |
|---|---|---|---|---|---|
| fcc | [$\bar{1}$10] | 0.79 | 1.95 | 4.69 | 5.47 |
| fcc | [$\bar{2}$11] | 0.67 | 1.95 | 4.57 | 5.39 |
| hcp | [$\bar{1}$10] | 0.79 | 1.96 | 4.71 | 5.61 |
| hcp | [$\bar{2}$11] | 0.73 | 1.96 | 4.65 | 5.55 |
| bridge | [$\bar{1}$10] | | 1.81 | | |
| bridge | [$\bar{2}$11] | 0.91 | 1.81 | 4.53 | |
| atop | [$\bar{1}$10] | | 1.59 | | |
| atop | [$\bar{2}$11] | | 1.59 | | |

[a] The two-phase adsorption energy is defined as the sum of the adsorption energies of Ni{111}/$C_6H_6$-$(\sqrt{7} \times \sqrt{7})$ [ref 16] and $2 \times$ Ni{111}/CO-$(\sqrt{3} \times \sqrt{3})$.

Similarly, we have considered the case of benzene coadsorption with CO, having first performed a new set of reference calculations for CO adsorbed on Ni{111} in the $(\sqrt{3} \times \sqrt{3})$ unit cell (our earlier work on Ni{111}/CO having been carried out for the relatively low-coverage $(2 \times 2)$ overlayer[17]). Once again, the *hcp* and *fcc* sites are strongly favored, suggesting that these are the only likely options for occupation in the coadsorbed system. Coadsorption in the *atop* and *bridge* sites is ruled out as before, on the grounds of the combination of separate adsorption energies (Table 2). Two-phase adsorption energies for the hollow site models fall in the range 4.57−4.71 eV per ($C_6H_6$ + 2CO) unit. The [$\bar{2}$11] *bridge* model is not quite so strongly unfavorable as was the case for O coadsorption, with a two-phase adsorption energy of 4.53 eV, but we nevertheless excluded it from further study in view of the fact that the DFT stability of the [$\bar{2}$11] *bridge* model for benzene in the $(\sqrt{7} \times \sqrt{7})$ structure is, if anything, overstated relative to the hollow sites.[19]


(7) Schaff, O.; Fernandez, V.; Hofmann, Ph.; Schindler, K.-M.; Theobald, A.; Fritzsche, V.; Bradshaw, A. M.; Davis, R.; Woodruff, D. P. *Surf. Sci.* **1996**, *348*, 89.
(8) Hohenberg, P.; Kohn, W. *Phys. Rev.* **1964**, *136*, B864.
(9) Kohn, W.; Sham, L. J. *Phys. Rev.* **1965**, *140*, A1133.
(10) CASTEP 4.2, academic version, licensed under the UKCP-MSI agreement, 1999−2004: Payne, M. C.; Teter, M. P.; Allan, D. C.; Arias, T. A.; Joannopoulos, J. D. *Rev. Mod. Phys.* **1992**, *64*, 1045.
(11) Vanderbilt, D. *Phys. Rev. B* **1990**, *41*, 1990.
(12) Perdew, J. P.; Chevary, J. A.; Vosko, S. H.; Jackson, K. A.; Pederson, M. R.; Singh, D. J.; Fiolhais, C. *Phys. Rev. B* **1992**, *46*, 6671.
(13) Monkhorst, H. J.; Pack, J. D. *Phys. Rev. B* **1976**, *13*, 5188.
(14) Louie, S. G.; Froyen, S.; Cohen, M. L. *Phys. Rev. B* **1982**, *26*, 1738.
(15) Jenkins, S. J. In *Computational Materials Science*; Leszczynski, J., Ed.; Elsevier: Amsterdam, 2004; Vol. 15.
(16) Yamagishi, S.; Jenkins, S. J.; King, D. A. *J. Chem. Phys.* **2001**, *114*, 5765.
(17) Karmazyn, A. D.; Fiorin, V.; Jenkins, S. J.; King, D. A. *Surf. Sci.* **2003**, *538*, 171.
(18) Yamagishi, S.; Jenkins, S. J.; King, D. A. *Surf. Sci.* **2003**, *543*, 12.
(19) *CRC Handbook of Chemistry and Physics*, 83rd ed.; Lide, D. R., Ed.; CRC Press: Boca Raton, FL, 2002.
(20) Bader, R. F. W. *Atoms in Molecules: A Quantum Theory*; Clarendon Press: Oxford, 1990.

***Table 3.*** Adsorption Energies (in eV per molecule) of CO on Ni{111} in the $(\sqrt{3} \times \sqrt{3})$ Structure[a]

| adsorption site | $(\sqrt{3}\times\sqrt{3})$ this work | $(\sqrt{3}\times\sqrt{3})$ [ref 23] | $(2\times2)$ [ref 20] |
|---|---|---|---|
| fcc | 1.95 | 1.93 | 2.02 |
| hcp | 1.96 | 1.94 | 2.05 |
| bridge | 1.81 | 1.81 | 1.90 |
| atop | 1.59 | 1.59 | 1.68 |

[a] Results of earlier DFT calculations for the $(\sqrt{3} \times \sqrt{3})$ [ref 23] and the $(2 \times 2)$ [ref 17] phases are listed for comparative purposes.

Table 3 lists energetic data for the pure CO adsorption system, for reference. Note that the adsorption energies of 1.96 and 1.95 eV per molecule, in the *hcp* and *fcc* sites respectively, are reasonably consistent with the 1.31 eV integral heat recorded at a 0.25 ML coverage in a single-crystal adsorption calorimetry (SCAC) experiment,[21] given the general tendency of DFT/PW91 to overbind molecules at metal surfaces.[22] The *hcp* site has also been reported as marginally the most stable in other DFT calculations of CO on Ni{111} in the $(\sqrt{3} \times \sqrt{3})$[23] and the $(2 \times 2)$[17] structures also shown in Table 3.

Looking in detail, for a moment, at the most favorable *hcp* model for the pure CO phase, the CO bond length and the height of the C atom above the surface plane are found to be 1.19 and 1.30 Å, respectively, in good agreement with values of 1.190 and 1.328 Å reported in previous DFT calculations.[23] The net electron flow is found to be 0.44 *e* in the direction from the surface to the molecule. We define a density difference function, $\Delta\rho_b^a(\mathbf{r})$, to represent the change in electron density when species "a" is adsorbed on substrate "b". That is,

$$\Delta\rho_{Ni}^{CO} = \rho_{Ni/CO} - \rho_{CO} - \rho_{Ni} \quad (1)$$

where the functional dependence on **r** has been suppressed for clarity; $\rho_{Ni/CO}$, $\rho_{CO}$, and $\rho_{Ni}$ represent the electron densities of CO on Ni{111}, gas-phase CO, and clean Ni{111}, respectively, all calculated with their constituent atoms frozen in the optimum geometries adopted upon adsorption. A plot of $\Delta\rho_{Ni}^{CO}$ (Figure 1A) reveals that the electron density increases in the region of the CO LUMO ($2\pi^*$) and decreases in the region of the CO HOMO ($5\sigma$). A plot of the residual spin density (i.e., $\rho_\alpha - \rho_\beta$) for the adsorption system demonstrates that the CO molecule gains a net minority spin (Figure 1B), which is distributed in the region of the LUMO, as found previously for both CO and NO on Ni{110}.[24,25] Previously published electron density difference and residual spin density plots for O on Ni{111}[18] are also shown in Figure 2 for comparative purposes.

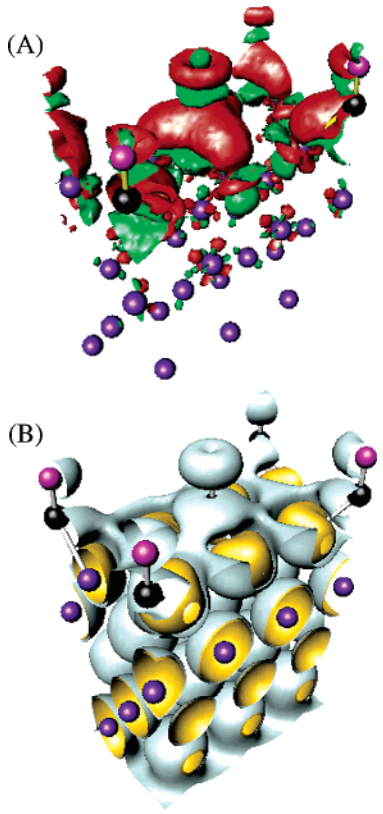


***Figure 1.*** (A) Density difference plot showing electron transfer upon adsorption of CO in the *hcp* sites of Ni{111} in the $(\sqrt{3} \times \sqrt{3})$ phase. Red contours indicate electron density decrease; green contours indicate electron density increase ($\pm 1.5 \times 10^{-2}$ Å$^{-3}$). (B) Residual spin density plot for the same system. Residual majority spin ($\rho_\alpha - \rho_\beta > 2.0 \times 10^{-3}$ Å$^{-3}$) shown in gold; residual minority spin ($\rho_\alpha - \rho_\beta < -2.0 \times 10^{-3}$ Å$^{-3}$) shown in silver.

## III. Results and Analysis

**A. Benzene Coadsorbed with O on Ni{111}. 1. Energetics.** Four models for coadsorption have been considered, in which O adatoms and benzene molecules occupy either *hcp* sites or *fcc* sites, with benzene in either the $[\bar{1}10]$ or the $[\bar{2}11]$ orientation. The *fcc* $[\bar{1}10]$ model was found to be the most favorable option, with a joint adsorption energy of 6.14 eV per $(C_6H_6 + 2O)$ unit, relative to the gas-phase molecular species (Table 1). This model is similar to that reported from the previous LEED experiment,[3] although it should be remembered that earlier ARUPS experiments had indicated the $[\bar{2}11]$ orientation.[2] It is interesting to note that the preference for the *fcc* adsorption site over the *hcp* site seems to be driven by the same preference exhibited by the pure O phase. The preference for the $[\bar{1}10]$ orientation appears to follow that of the pure benzene phase hollow site models.[16]

To estimate the interactions between the adsorbates, we also performed separate calculations of (i) benzene with the $[\bar{1}10]$ orientation on the *fcc* site of Ni{111} and (ii) 2O on the *fcc* site of Ni{111}, both within the same $(2\sqrt{3} \times 2\sqrt{3})R30°$ unit cell as in the coadsorption system (see Figure 3 for the disposition of adsorbates within the unit cell). We obtained the adsorption energies of these systems as (i) 1.23 eV relative to gas-phase benzene and (ii) 4.93 eV relative to gas-phase $O_2$. There is thus essentially no net energy of interaction between the benzene and the oxygen adatoms in the coadsorbed system (the sum of these separate adsorption energies is only 0.02 eV larger than the joint adsorption energy of the coadsorption system). We might therefore ask what the driving force for the formation of a mixed benzene/oxygen phase could be, in the absence of an attractive interspecies interaction. The answer may be found by considering the saturated islands of $(\sqrt{7} \times \sqrt{7})$ benzene and $(\sqrt{3} \times \sqrt{3})$ oxygen phases which constitute the alternative to intimate coadsorption.

We take, as our starting point, a surface on which benzene molecules and O adatoms are deposited at the appropriate density to form a perfect coadsorbed overlayer but are arranged instead in separate islands at close to saturation local coverage (see Figure 4). Ignoring edge effects, the integral adsorption energies for these islands may be taken from our previous

(21) Stuckless, J. T.; Al-Sarraf, N.; Wartnaby, C.; King, D. A. *J. Chem. Phys.* **1993**, *99*, 2202.
(22) Ge, Q.; Kose, R.; King, D. A. *Adv. Catal.* **2001**, *43*, 207.
(23) Eichler, A. *Surf. Sci.* **2003**, *526*, 332.
(24) Ge, Q.; Jenkins, S. J.; King, D. A. *Chem. Phys. Lett.* **2000**, *327*, 125.
(25) Jenkins, S. J.; Ge, Q.; King, D. A. *Phys. Rev. B* **2001**, *64*, 012413.

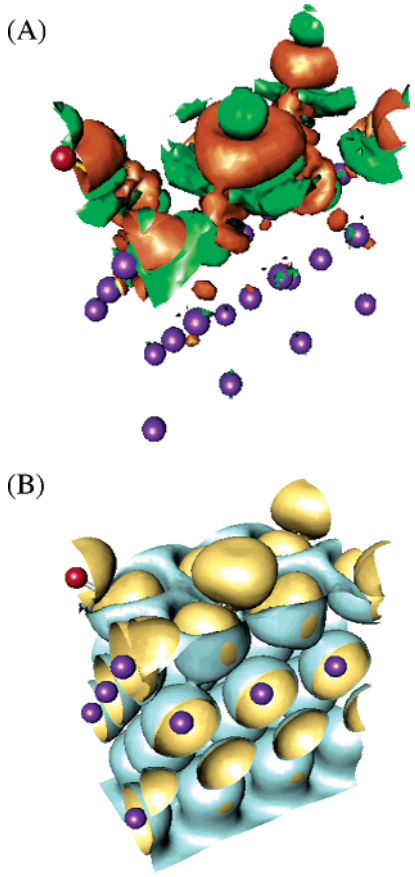


***Figure 2.*** (A) Density difference plot showing electron transfer upon adsorption of O in the *hcp* sites of Ni{111} in the ($\sqrt{3} \times \sqrt{3}$) phase. (B) Residual spin density plot ($\rho_\alpha - \rho_\beta$) for the same system. Color scheme and isosurface threshold values as defined in Figure 1.

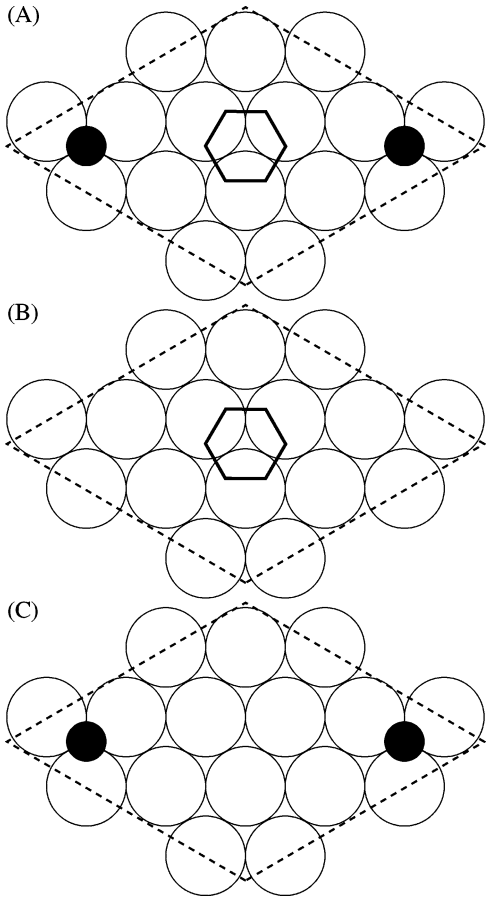


***Figure 3.*** Schematics of the ($2\sqrt{3} \times 2\sqrt{3}$) unit cells of $C_6H_6$ coadsorbed with (A) O/CO, (B) $C_6H_6$, and (C) 2O/2CO on Ni{111}, respectively.

calculations for benzene[16] and oxygen[18] adsorption. Simply diluting the saturated bridge-adsorbed ($\sqrt{7} \times \sqrt{7}$) benzene islands (in the absence of oxygen) to the ($2\sqrt{3} \times 2\sqrt{3}$) density and *fcc* site appropriate for the coadsorbed phase (case (i) above) produces an increase in adsorption energy of 0.32 eV per molecule. Similarly, diluting the saturated ($\sqrt{3} \times \sqrt{3}$) oxygen islands (in the absence of benzene) to a ($2\sqrt{3} \times 2\sqrt{3}$) structure compatible with the coadsorbed phase (case (ii) above) produces an increase in adsorption energy of 0.71 eV per 2O adatoms. The reduction of repulsive interactions between neighboring benzene molecules, and particularly between neighboring O adatoms, essentially accounts almost perfectly for the 1.01 eV increase in calculated adsorption energy for the coadsorbed system compared with the sum of the separate adsorption energies for pure saturated overlayers. Thus it is the reduction in intraspecies repulsive interactions which is the driving force for the formation of the intimately coadsorbed phase and not any attractive interspecies interactions (Figure 4). The interspecies interactions are actually mildly repulsive at this joint coverage but far less so than the intraspecies interactions in the saturated single-species overlayers.

**2. Structural Analysis.** The calculated geometry of the *fcc* [$\bar{1}$10] model of benzene coadsorbed with O on Ni{111} is shown in Figure 5. The top Ni layer shows a strong buckling of 0.20 Å, with those atoms beneath the molecule being raised somewhat out of the surface. This buckling is larger than that reported in the previous LEED experiment (0.04 Å),[3] but similar differences between LEED and DFT were found in previous studies of pure benzene on Ni{111}.[16,26] The second layer also buckles slightly in our calculations, by 0.05 Å, and the perpendicular distance between the C atoms and the highest-lying Ni atoms is found to be 1.97 Å, in good agreement with the LEED experiment (1.94 Å). The radius of the benzene ring is slightly expanded, with C−C bond lengths of 1.41 and 1.43 Å, compared to gas-phase values of 1.381 Å (theory[16]) and 1.399 Å (experiment[19]). These results are in acceptable agreement with the LEED experiment, which shows C−C bond lengths of 1.42 and 1.36 Å, bearing in mind that LEED experiments typically show less precision in lateral than vertical geometrical analysis. The H atoms of benzene, which were not included in the LEED study, rise up to make angles with the surface plane of 16.4°. The corresponding C−H bond lengths are 1.08 Å, virtually unchanged from the gas-phase results of 1.08 Å (theory[16]) and 1.101 Å (experiment[19]).

The perpendicular distance between the O atoms and the highest-lying Ni atoms was found to be 1.00 Å, which is rather less than the result of the LEED experiment (1.25 and 1.30 Å). The two O atoms in each unit cell are found to buckle in the LEED analysis; we have not allowed such buckling to occur, for reasons of computational economy, but it is unlikely that this would entirely account for the discrepancy. There is thus a clear disagreement between LEED, which shows the O atoms raised by 0.17 and 0.22 Å, relative to a ($\sqrt{3} \times \sqrt{3}$) height of

(26) Mittendorfer, F.; Hafner, J. *Surf. Sci.* **2001**, *472*, 133.

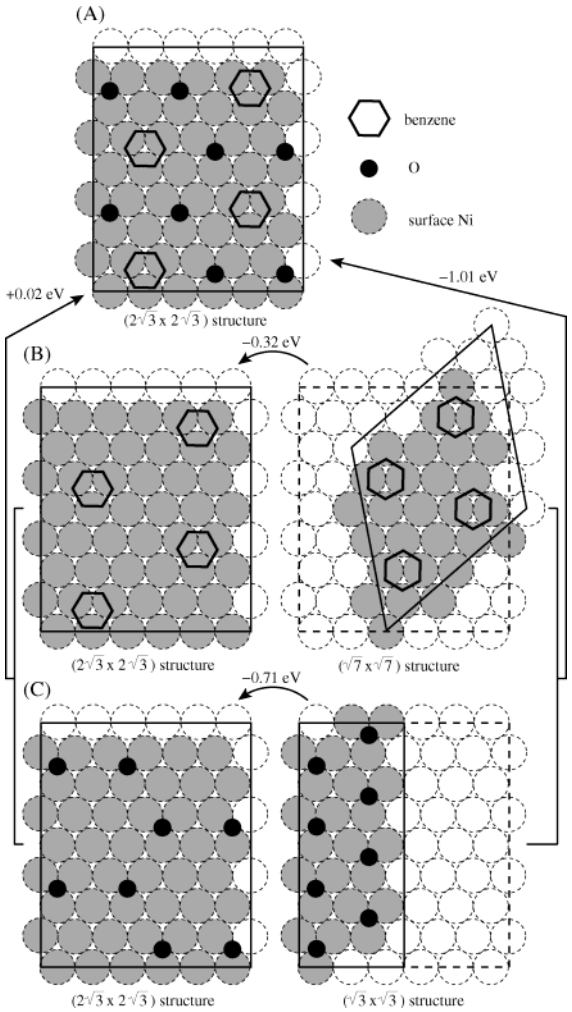


***Figure 4.*** Schematic of energy changes upon adsorbate rearrangement for $C_6H_6$ and 2O on Ni{111}. Marked energy changes are to be understood as being per $C_6H_6$, per 2O or per ($C_6H_6$ + 2O) unit, as appropriate.

1.08 Å, and the DFT result, which shows them lowered by 0.14 Å, relative to a ($\sqrt{3} \times \sqrt{3}$) height of 1.14 Å.

**3. Electron and Spin Density Analysis.** We commence our analysis of the electron density by defining a density difference function for the coadsorbed system as

$$\Delta\rho_{Ni}^{C_6H_6+2O} = \rho_{Ni/(C_6H_6+2O)} - \rho_{C_6H_6} - \rho_{2O} - \rho_{Ni} \qquad (2)$$

where $\rho_{Ni/(C_6H_6+2O)}$, $\rho_{Ni/2O}$, and $\rho_{Ni/C_6H_6}$ represent the electron densities of coadsorbed and separately adsorbed benzene molecules and O adatoms, with the systems frozen in the optimum geometries established for the coadsorbed case; $\rho_{2O}$ and $\rho_{C_6H_6}$ represent gas-phase electron densities for oxygen atoms and benzene molecules, again frozen in the optimum coadsorption geometries. The $\Delta\rho_{Ni}^{C_6H_6+2O}$ function thus indicates the total change in electron density which occurs when both species are deposited onto the clean surface. Plots of this function for the *fcc* [$\bar{1}$10] and [$\bar{2}$11] models are shown in Figure 6A and Figure 7A, respectively. In these figures, the benzene molecules and the O adatoms appear almost the same as in our previous studies of pure benzene on Ni{111}[16] and pure O on Ni{111}.[18] Similarly, plots of residual spin density (i.e., $\rho_\alpha - \rho_\beta$) are also reminiscent of those for the individual species (Figure 6B and Figure 7B). In both models, we note that the

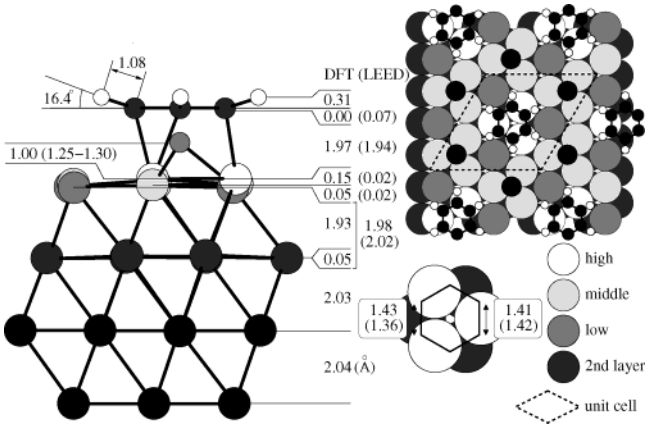


***Figure 5.*** Detailed geometry of $C_6H_6$/2O coadsorption at the *fcc* site of Ni{111}. Distances calculated in the present work are given in Å units, as are the results of the previous LEED [ref 3] experiment (in parentheses).

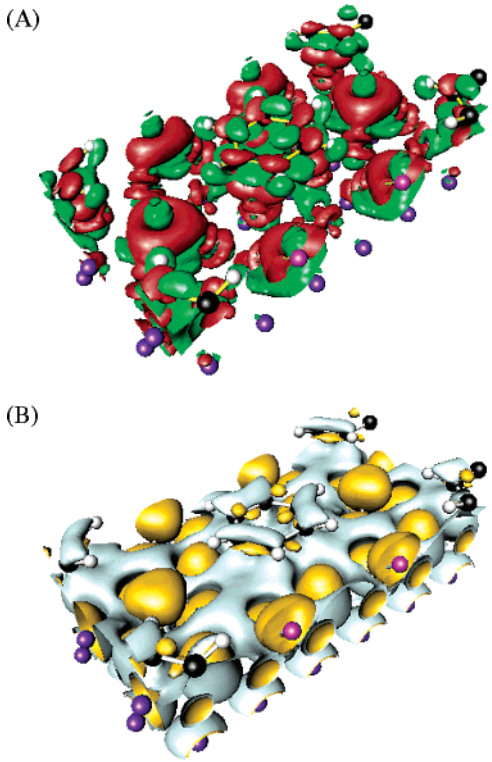


***Figure 6.*** (A) Density difference plot showing electron transfer upon coadsorption of $C_6H_6$ and O in the *fcc* [$\bar{1}$10] model. (B) Residual spin density plot ($\rho_\alpha - \rho_\beta$) for the same system. Color scheme and isosurface threshold values as defined in Figure 1.

adsorbed O atoms show a net majority spin and that the electron density increases in the $2p_x$ and $2p_y$ orbitals and decreases in the $2p_z$ orbitals. On the other hand, the adsorbed benzene gains a net minority spin and reflects a Kekule-like symmetry in the *fcc* [$\bar{1}$10] model and C $2p_z$-like lobes in the *fcc* [$\bar{2}$11] model.

To understand the changes in electron density upon coadsorption, we define two further density difference functions as follows:

$$\Delta\rho_{Ni/2O}^{C_6H_6} = \rho_{Ni/(C_6H_6+2O)} - \rho_{C_6H_6} - \rho_{Ni/2O} \qquad (3)$$

$$\Delta\rho_{Ni/C_6H_6}^{2O} = \rho_{Ni/(C_6H_6+2O)} - \rho_{2O} - \rho_{Ni/C_6H_6} \qquad (4)$$

The $\Delta\rho_{Ni/2O}^{C_6H_6}$ and $\Delta\rho_{Ni/C_6H_6}^{2O}$ functions thus indicate the changes in electron density which would occur upon adsorption

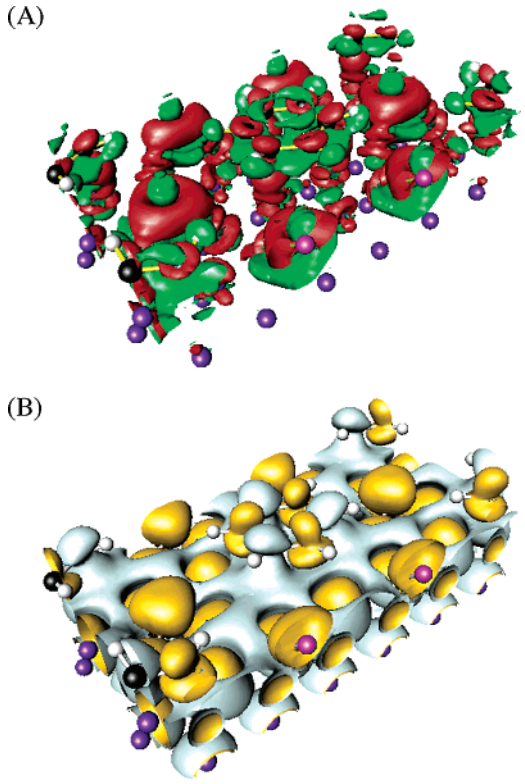


***Figure 7.*** (A) Density difference plot showing electron transfer upon coadsorption of $C_6H_6$ and O in the *fcc* [$\bar{2}11$] model. (B) Residual spin density plot ($\rho_\alpha - \rho_\beta$) for the same system. Color scheme and isosurface threshold values as defined in Figure 1.

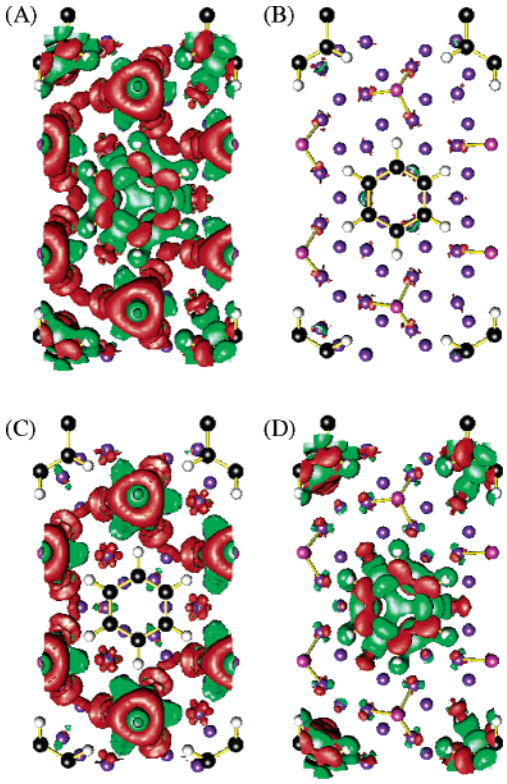


***Figure 8.*** Charge density difference plots of (A) $\Delta\rho_{Ni}^{C_6H_6+2O}$; (B) $\Delta\rho_{Ni/(C_6H_6+2O)}$; (C) $\Delta\rho_{Ni/C_6H_6}^{2O}$; and (D) $\Delta\rho_{Ni/2O}^{C_6H_6}$. Color scheme and isosurface threshold values as defined in Figure 1.

of each species on a surface already precovered by its coadsorbate. In addition, we define a final density difference function, $\Delta\rho_{Ni/(C_6H_6+2O)}$, which represents the change in electron density occurring when separate islands of adsorbed benzene molecules and adsorbed O adatoms are rearranged to form islands of the coadsorbed phase and complementary patches of clean surface:

$$\Delta\rho_{Ni/(C_6H_6+2O)} = \rho_{Ni/(C_6H_6+2O)} + \rho_{Ni} - \rho_{Ni/C_6H_6} - \rho_{Ni/2O} \quad (5)$$

Plots of these supplementary density difference functions (Figures 8 and 9) reveal that (i) the density difference for O adsorption in the presence of preadsorbed benzene, $\Delta\rho_{Ni/C_6H_6}^{2O}$, is very little different from that in the absence of benzene; (ii) the density difference for benzene adsorption in the presence of preadsorbed O adatoms, $\Delta\rho_{Ni/2O}^{C_6H_6}$, is very little different from that in the absence of O adatoms; and (iii) the density change when well-separated adsorbed benzene molecules and O adatoms are brought into close proximity, $\Delta\rho_{Ni/(C_6H_6+2O)}$, is very small in relation to the changes occurring during adsorption.

To analyze the localized properties of our calculated results, the topological method introduced by Bader[20] has been employed. The surfaces of zero normal gradient in the charge density field provide a unique and conceptually appealing criterion for partitioning charge among the atoms at the surface. This method has recently proved extremely useful in extracting localized information from plane wave surface calculations.[16,24,27−31] In this way, we investigated atom-resolved charges and magnetic moments of the *fcc* [$\bar{1}10$] model shown in Table 4. The net electron flow is from Ni to the adsorbed benzene (0.29 *e*/molecule) and to the O adatoms (0.92 *e*/O). Although the electron transfer from Ni to O increases by 0.06 *e* compared to the ($\sqrt{3} \times \sqrt{3}$) phase, that from Ni to benzene decreases by 0.18 *e* compared to the ($\sqrt{7} \times \sqrt{7}$) phase (in the preferred *bridge* [$\bar{2}11$] model).

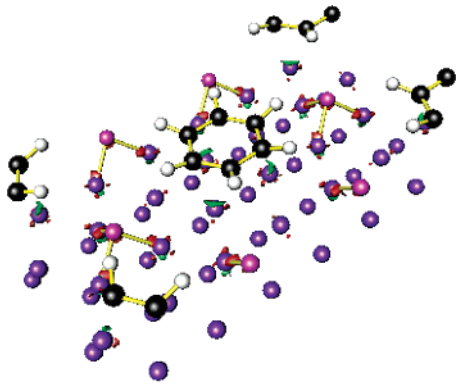

***Figure 9.*** Density difference plot of $\Delta\rho_{Ni/(C_6H_6+2O)}$ (as Figure 8B, but oblique view). Color scheme and isosurface threshold values as defined in Figure 1.

**B. Benzene Coadsorbed with CO on Ni{111}. 1. Energetics.** Four models for the coadsorption of benzene with CO were calculated, corresponding to occupancy of the *fcc* and *hcp* sites, with [$\bar{1}10$] and [$\bar{2}11$] orientations for the benzene molecules.

(27) Jenkins, S. J.; King, D. A. *Chem. Phys. Lett.* **2000**, *317*, 381.
(28) Jenkins, S. J.; King, D. A. *J. Am. Chem. Soc.* **2000**, *122*, 10610.
(29) Held, G.; Braun, W.; Steinrück, H.-P.; Yamagishi, S.; Jenkins, S. J.; King, D. A. *Phys. Rev. Lett.* **2001**, *87*, 216102.
(30) Yamagishi, S.; Jenkins, S. J.; King, D. A. *J. Chem. Phys.* **2002**, *117*, 819.
(31) Yamagishi, S.; Jenkins, S. J.; King, D. A. *Chem. Phys. Lett.* **2003**, *367*, 116.

***Table 4.*** Atom-Resolved Charges, $q$, and Magnetic Moments, $\mu$, for Ni{111}/$C_6H_6$-($\sqrt{7} \times \sqrt{7}$) [ref 16], Ni{111}/O-($\sqrt{3} \times \sqrt{3}$) [ref 18] and Ni{111}/($C_6H_6$ + 2O)-($2\sqrt{3} \times 2\sqrt{3}$)[a]

| | Ni{111}/$C_6H_6$ | | Ni{111}/O | | Ni{111}/($C_6H_6$+2O) | |
|---|---|---|---|---|---|---|
| | charge | spin | charge | spin | charge | spin |
| Ni (Type I) | 0.11 | 0.31 | | | 0.13 | 0.43 |
| Ni (Type II) | 0.02 | 0.64 | | | 0.07 | 0.68 |
| Ni (Type III) | | | 0.28 | 0.53 | 0.23 | 0.53 |
| $C_6H_6$ | −0.47 | −0.04 | | | −0.29 | −0.05 |
| O | | | −0.86 | 0.16 | −0.92 | 0.12 |

[a] Units are the electronic charge, $e$, and the Bohr magneton, $\mu_B$, respectively. Type I Ni atoms bond with $C_6H_6$, type II form no bonds, and type III form bonds with O. For comparison, the Ni atoms at the clean Ni{111} surface are calculated to have $q = -0.02e$ and $\mu = 0.68\mu_B$ [ref 16].

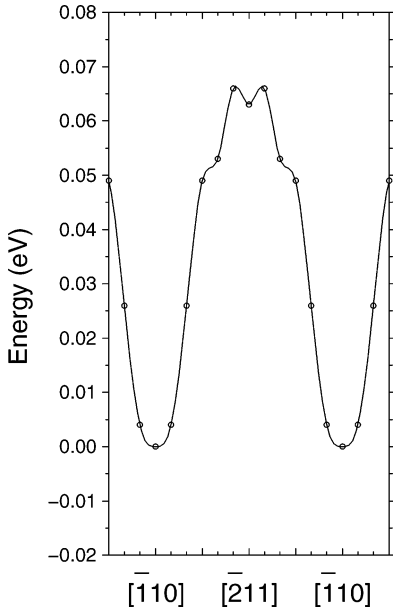


***Figure 10.*** Azimuthal angular dependence of energy for coadsorbed $C_6H_6$ and 2CO on Ni{111}. Energy is measured per ($C_6H_6$ + 2CO) unit, referenced to the value in the [110] model, and the curve is merely a guide to the eye.

The *hcp* [$\bar{1}$10] model was found to be the most favorable option, with an adsorption energy of 5.61 eV per ($C_6H_6$ + 2CO) unit (Table 2). The preferred site is in agreement with the previous LEED experiment.[5,6] Although the *hcp* site is the same as that preferred by pure CO on Ni{111}, the energy difference over the *fcc* site is substantially greater in the coadsorbed system. The preference for the [$\bar{1}$10] orientation once again appears to follow the preference of the pure benzene phase, but is not in agreement with the [$\bar{2}$11] orientation found in the LEED[5,6] and ARUPS[2,4] studies.

In view of the small energy difference between the two orientations, we carried out a series of calculations in which the benzene molecule was gradually rotated in 5° steps, its internal lateral coordinates being fixed at an appropriate linear interpolation between the two fully relaxed end points. All other atomic degrees of freedom were allowed to relax as before, and the resulting energy curve is displayed in Figure 10. The [$\bar{2}$11] orientation appears as a shallow minimum in the raw data, although the barrier preventing rotation into the [$\bar{1}$10] orientation is revealed as around 0.005 eV, not reliable within the accuracy of the present calculations. Fitting a polynomial to the results close to the [$\bar{1}$10] orientation, one may estimate a rigid rotational frequency of around 35 $cm^{-1}$ for $C_6H_6$ or 31 $cm^{-1}$ for $C_6D_6$. Such frequencies are substantially lower than those calculated previously for pure benzene overlayers on Ru{0001}[29] of 78 and 71 $cm^{-1}$ respectively, although it seems unlikely that even such slow oscillations could account for the discrepancy between experiment and theory in this case.

As in the case of coadsorption with oxygen, we investigated the interactions between the adsorbates by performing separate calculations of (i) benzene with the [$\bar{1}$10] orientation in the *hcp* site of Ni{111} and (ii) 2CO on the *hcp* site of Ni{111}, both within the same ($2\sqrt{3} \times 2\sqrt{3}$)*R*30° unit cell as for the coadsorption system (see Figure 3). We obtained the adsorption energies of these systems as (i) 1.28 eV and (ii) 4.03 eV. In contrast to the benzene/oxygen coadsorption system, there is clearly a net energy of interaction between the benzene and CO molecules, because the adsorption energy of the coadsorption system is 0.30 eV larger than the sum of the separate adsorption energies.

Considering dilution of saturated bridge-adsorbed ($\sqrt{7} \times \sqrt{7}$) benzene islands (in the absence of CO) to the ($2\sqrt{3} \times 2\sqrt{3}$) density of the coadsorbed phase (case (i) above) produces an increase in adsorption energy of 0.37 eV per molecule. This differs from the value used in our discussion of coadsorption with oxygen because the final state here is the *hcp* adsorption site, rather than the *fcc*. Dilution of ($\sqrt{3} \times \sqrt{3}$) CO islands (in the absence of benzene) to a ($2\sqrt{3} \times 2\sqrt{3}$) structure compatible with the coadsorbed phase (case (ii) above) produces an increase in adsorption energy of only 0.11 eV per 2CO molecules (compared with 0.71 eV per 2O adatoms in the case of oxygen). Thus the increase in adsorption energy of 0.78 eV for the coadsorbed phase relative to the sum of the separate adsorption energies for the pure islands has very little to do with repulsive interaction between CO molecules. The driving force for the formation of the intimately coadsorbed phase is therefore predominantly a combination of intraspecies repulsion between benzene molecules and interspecies attraction between benzene and CO molecules (see Figure 11).

Note that the ($2\sqrt{3} \times 2\sqrt{3}$) ordered coadsorption structure was reported to be formed at room temperature,[5,6,32] so we should strictly discuss the energetics of the pure CO phase with reference to the 0.25 ML saturated $c(2 \times 4)$ structure[32] formed under the same conditions. Previous DFT studies, however, have shown that the adsorption energies of CO in the hollow sites of Ni{111} are fairly constant in the coverage range between 0.1 and 0.5 ML.[23] We therefore use the ($\sqrt{3} \times \sqrt{3}$) model, with confidence that the energetics are almost identical, for ease of comparison with the results for benzene/oxygen coadsorption.

**2. Structural Analysis.** The calculated geometry of the *hcp* [$\bar{1}$10] model of benzene coadsorbed with CO on Ni{111} is shown in Figure 12. The top Ni layer shows a strong buckling of 0.19 Å, with those atoms beneath the molecule being raised somewhat out of the surface, again rather larger than the buckling reported in LEED experiments (0.04 Å).[5,6] The second layer also buckles in our calculations, by 0.14 Å which is in good agreement with the LEED study (0.15 Å), and the perpendicular distance between the lowest-lying C atoms of the benzene molecule and the highest-lying Ni atoms is found to be 1.97 Å, which is almost the same as that in the LEED

(32) Held, G.; Schuler, J.; Sklarek, W.; Steinrück, H.-P. *Surf. Sci.* **1998**, *217*, 154.

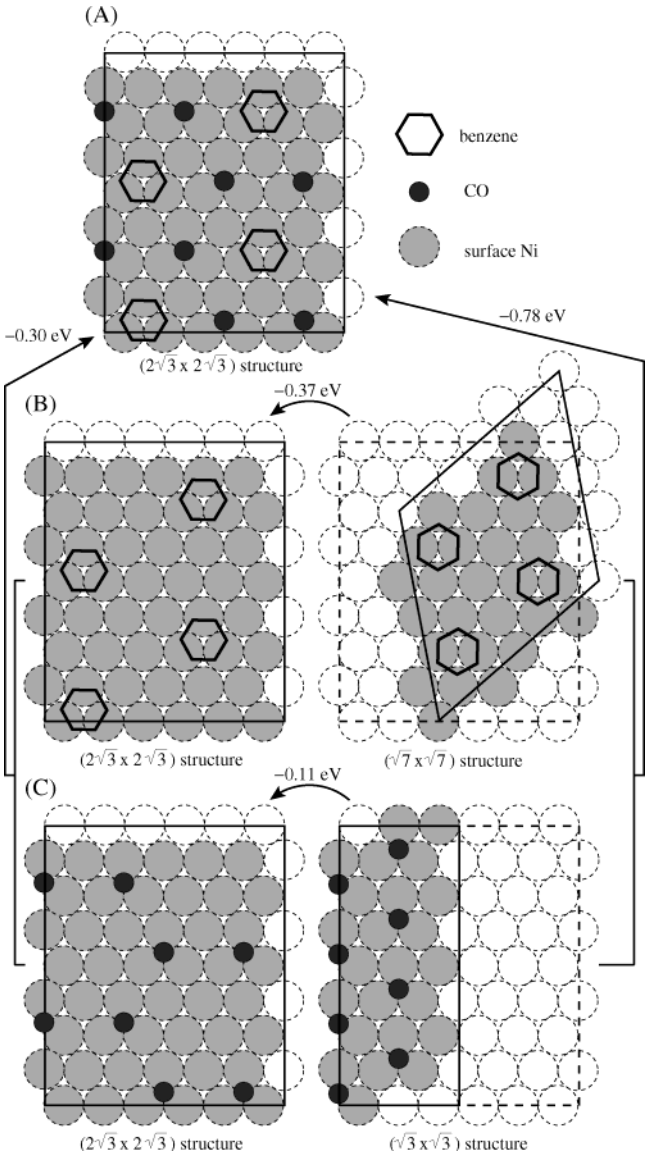


***Figure 11.*** Schematic of energy changes upon adsorbate rearrangement for $C_6H_6$ and 2CO on Ni{111}. Marked energy changes are to be understood as being per $C_6H_6$, per 2CO, or per ($C_6H_6$ + 2CO) unit, as appropriate.

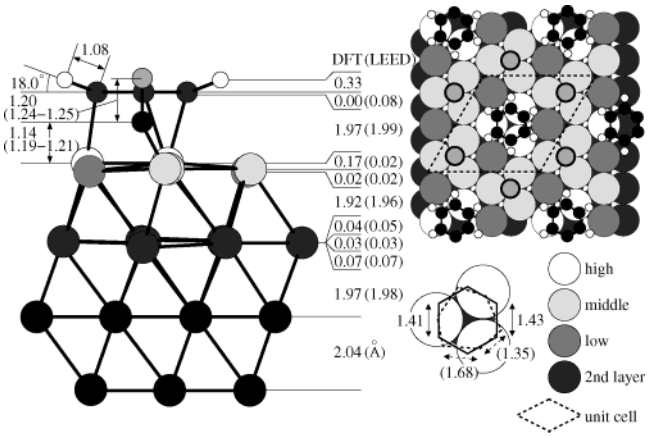


***Figure 12.*** Detailed geometry of $C_6H_6$/2CO coadsorption at the *hcp* site of Ni{111}. Distances calculated in the present work are given in Å units, as are the results of the previous LEED [ref 5] experiment (in parentheses).

experiment (1.97 Å). The radius of the benzene molecule is also slightly expanded, with C−C bond lengths of 1.41 and 1.43 Å. On the other hand, in the LEED experiment the benzene molecule is oriented in the [$\bar{2}$11] direction and strongly distorted, with C−C bond lengths of 1.35 and 1.68 Å. It should be noted that all the C−C bond lengths of our *hcp* [$\bar{2}$11] model are 1.42 Å in length and that a 3-fold rotational symmetry has been imposed. We believe that the highly distorted geometry obtained in LEED may be an artifact and that this may also account for the difference in apparent benzene orientation between LEED and DFT. The H atoms of the benzene molecule, which were not included in the LEED study, rise upward to make angles of 18.0° with the surface plane. The corresponding C−H bond lengths are 1.08 Å, virtually unchanged from the gas-phase results of 1.084 Å (theory[16]) and 1.101 Å (experiment[19]).

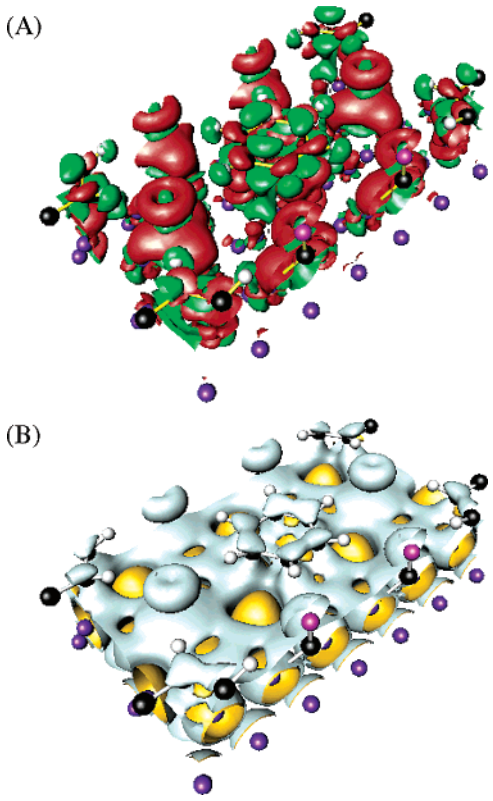


***Figure 13.*** (A) Density difference plot showing electron transfer upon coadsorption of $C_6H_6$ and CO in the *hcp* [$\bar{1}$10] model. (B) Residual spin density plot ($\rho_\alpha - \rho_\beta$) for the same system. Color scheme and isosurface threshold values as defined in Figure 1.

The C−O bond length is expanded to 1.20 Å from the calculated gas-phase value of 1.14 Å, in passable agreement with the findings of the LEED study (1.24 and 1.25 Å for two inequivalent CO molecules). The calculated C−O bond length of pure CO on Ni{111} in the ($\sqrt{3} \times \sqrt{3}$) phase is 1.19 Å, which is only slightly less than that in the coadsorption system. The perpendicular distance between the C atom of the CO molecule and the highest-lying Ni atoms is found to be 1.14 Å, which is less than the result of the LEED experiment (1.19 and 1.21 Å). The CO of the coadsorption system is adsorbed on the surface more closely than that in the pure CO ($\sqrt{3} \times \sqrt{3}$)-phase, where DFT gave a vertical distance of 1.30 Å.

**3. Electron and Spin Density Analysis.** Electron density difference plots, showing $\Delta\rho_{Ni}^{C_6H_6+2CO}$ for *hcp* [$\bar{1}$10] and [$\bar{2}$11] models are presented in Figures 13A and 14A, respectively. In these figures, the benzene and CO molecules appear almost the same as in the studies of pure benzene on Ni{111}[16] and pure

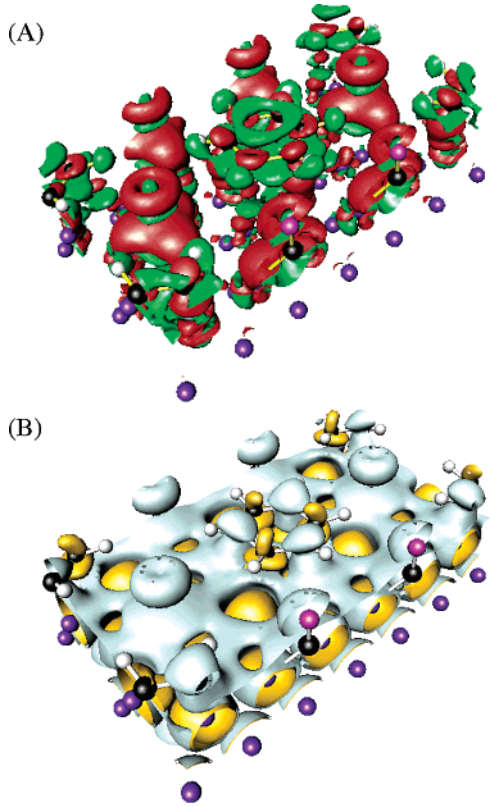


***Figure 14.*** (A) Density difference plot showing electron transfer upon coadsorption of $C_6H_6$ and CO in the *hcp* [$\bar{2}11$] model. (B) Residual spin density plot ($\rho_\alpha - \rho_\beta$) for the same system. Color scheme and isosurface threshold values as defined in Figure 1.

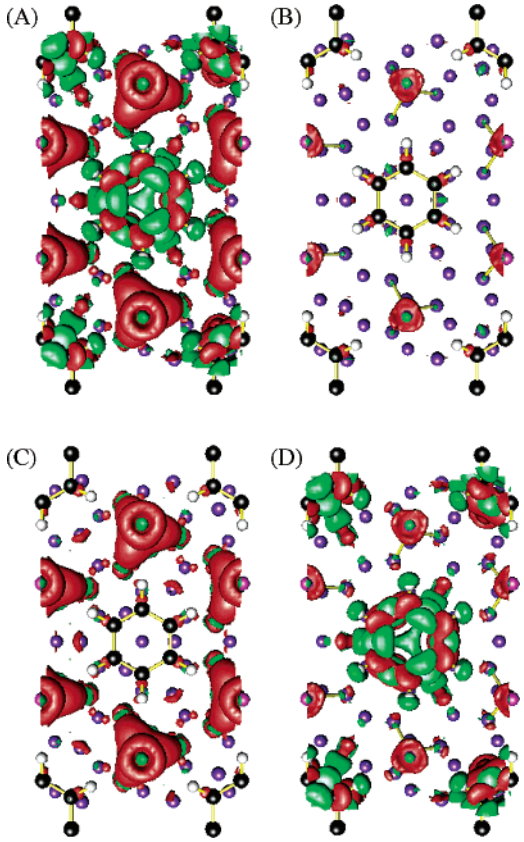


***Figure 15.*** Charge density difference plots of (A) $\Delta\rho_{Ni}^{C_6H_6+2CO}$; (B) $\Delta\rho_{Ni/(C_6H_6+2CO)}$; (C) $\Delta\rho_{Ni/C_6H_6}^{2CO}$; and (D) $\Delta\rho_{Ni/2CO}^{C_6H_6}$. Color scheme and isosurface threshold values as defined in Figure 1.

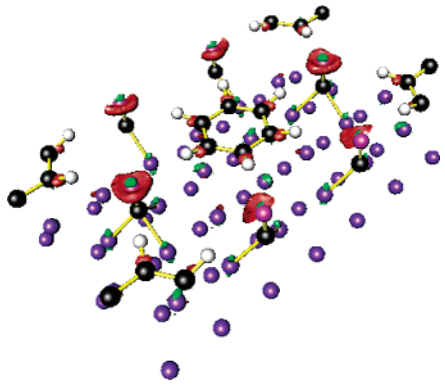

***Figure 16.*** Density difference plot of $\Delta\rho_{Ni/(C_6H_6+2CO)}$ (as Figure 15B, but oblique view). Color scheme and isosurface threshold values as defined in Figure 1.

CO on Ni{111} (see Figure 1). Residual spin density plots (i.e., $\rho_\alpha - \rho_\beta$) are likewise very similar to the noncoadsorbed cases (Figures 13B and 14B). We also plotted (Figures 15 and 16) electron density difference functions $\Delta\rho_{Ni/2CO}^{C_6H_6}$, $\Delta\rho_{Ni/C_6H_6}^{2CO}$, and $\Delta\rho_{Ni/(C_6H_6+2CO)}$, defined by analogy with the corresponding functions in eqs 3−5. Compared with the case of $C_6H_6$/2O coadsorption, the electron density changes induced in the vicinity of the O atoms by the proximity of the benzene molecules are far more pronounced, in line with our conclusion above that attractive interspecies interactions play a significant role in stabilizing the $C_6H_6$/2CO system.

We investigated atom-resolved charges and magnetic moments of the *hcp* [$\bar{1}10$] model shown in Table 5. The net electron flow is from Ni to the adsorbed benzene (0.22 *e*/molecule) and the CO (0.58 *e*/molecule). Although the electron transfer from Ni to CO increases by 0.14 *e* compared to the ($\sqrt{3} \times \sqrt{3}$) phase, that from Ni to benzene decreases by 0.25 *e* compared to the ($\sqrt{7} \times \sqrt{7}$)-benzene phase (the *bridge* [$\bar{2}11$] model).

## IV. Discussion and Conclusions

Our DFT calculations for the ($2\sqrt{3} \times 2\sqrt{3}$)*R*30° phases of ($C_6H_6$ + 2O) and($C_6H_6$ + 2CO) confirm the experimental finding of *fcc* occupancy in the former case and *hcp* occupancy in the latter. The determining factor appears to be the site preference of the nonaromatic adsorbate, by virtue of its more site specific adsorption energy. Averaging over the two different high-symmetry orientations of the benzene molecule, the energy difference between *hcp* and *fcc* sites amounts to a credible 0.17 eV in the case of coadsorption with O adatoms and 0.15 eV in the case of coadsorption with CO molecules. The site specificity of the present calculations is thus expected to be relatively secure.

In contrast, the energy difference between differing orientations of the benzene molecule is found to be somewhat smaller (verging upon negligible in the context of probable error margins). The trend is always to favor the [$\bar{1}10$] orientation of the benzene molecule over the [$\bar{2}11$] orientation, for a given site and coadsorbate, but by only 0.06−0.12 eV. Photoemission and crystallographic experiments, however, tend to favor the [$\bar{2}11$] orientation,[2,4−6] with the exception of a LEED study on the ($C_6H_6$ + 2O) overlayer.[3] It seems that the balance between the different molecular orientations is probably rather fine and sensitive not only to variations in the experimental conditions

***Table 5.*** Atom-Resolved Charges, $q$, and Magnetic Moments, $\mu$, for Ni{111}/$C_6H_6$-($\sqrt{7} \times \sqrt{7}$) [ref 16], Ni{111}/CO-($\sqrt{3} \times \sqrt{3}$) and Ni{111}/($C_6H_6$ + 2CO)-($2\sqrt{3} \times 2\sqrt{3}$)[a]

| | Ni{111}/$C_6H_6$ | | Ni{111}/CO | | Ni{111}/($C_6H_6$+2CO) | |
|---|---|---|---|---|---|---|
| | charge | spin | charge | spin | charge | spin |
| Ni (Type I) | 0.11 | 0.31 | | | 0.12 | 0.34 |
| Ni (Type II) | 0.02 | 0.64 | | | 0.07 | 0.63 |
| Ni (Type III) | | | 0.14 | 0.14 | 0.11 | 0.32 |
| $C_6H_6$ | −0.47 | −0.04 | | | −0.22 | −0.05 |
| CO | | | −0.44 | −0.04 | −0.58 | −0.07 |

[a] Units are the electronic charge, $e$, and the Bohr magneton, $\mu_B$, respectively. Type I Ni atoms bond with $C_6H_6$, type II form no bonds, and type III form bonds with CO.

but also perhaps to subtle isotope effects beyond the scope of the present calculations. In this regard, it is worth noting that the ARUPS measurements[2,4] and one of the LEED studies[5,6] were actually performed with $C_6D_6$, while the other LEED study[3] used $C_6H_6$.

Site and orientation preferences aside, however, the crucial insight offered by the present DFT calculations is that the self-organization of the coadsorbates in the two different overlayers arises from two different effects. In the case of the ($C_6H_6$ + 2O) overlayer, it is the strong repulsion between the O adatoms which provides the primary driving force toward formation of an intimate ordered structure. The repulsion between $C_6H_6$ molecules provides a secondary contribution, while the interaction energy between the coadsorbed species in the ordered overlayer is practically nil. In contrast, the tendancy toward formation of an intimate ordered overlayer in the ($C_6H_6$ + 2CO) case is driven in almost equal measure by the repulsion between $C_6H_6$ molecules and by the attractive energy of interaction between the coadsorbates in the ordered overlayer. The repulsion between CO molecules plays only a minor role.

In conclusion, therefore, we have shown that the present DFT calculations allow a detailed understanding of self-organization in benzene coadsorption systems. The picture that emerges is one in which the site preferences are determined by the nonaromatic species, the orientational preferences are finely balanced, and the tendency toward long-range order may be induced *either* through the intraspecies repulsive interactions of the coadsorbates *or* through their interspecies attractions.

**Acknowledgment.** We acknowledge financial support for this work from the EPSRC(UK), in the form of funds for workstations and a postdoctoral assistantship (S.Y.). One of us (S.J.J.) would like to thank The Royal Society for a University Research Fellowship. The main calculations were carried out on the IBM SP3 machine at the Cambridge-Cranfield High Performance Computing Facility.

JA048289Y